Theor Chem Acc (2013) 132:1383
DOI 10.1007/s00214-013-1383-3

REGULAR ARTICLE

DFT insight into *o*-semiquinone radicals and Ca^{2+} ion interaction: structure, *g* tensor, and stability

Maciej Witwicki · Julia Jezierska

Received: 4 April 2013 / Accepted: 12 July 2013 / Published online: 30 July 2013

Abstract Density functional theory methods were employed to elucidate the interactions between calcium ions and various *o*-semiquinone radicals mimicking the interactions occurring in biochemical systems. Predicted changes in the molecular and electronic structures of the radicals on Ca^{2+} coordination were correlated with the changes of *g* tensor and compared with those exerted by Mg^{2+} ions (reported by us previously). In order to broaden the insight into the differences between the Mg^{2+} and Ca^{2+} complexes, their relative stability was estimated on the basis of theoretically predicted Gibbs energies for the process of the complex formation.

Keywords EPR · ESR · Semiquinone radicals · Paramagnetic complexes · Radical ligands

1 Introduction

Organic radical ions play increasingly important roles in modern biochemistry and material science [1, 2]. Semiquinones are typical organic radical anions being the intermediate form in the redox equilibrium between quinones and hydroquinones. These radicals are present in all life forms as they act as electron-transfer agents in the mitochondrial respiratory chain and in the reaction centers of bacterial and plant photosynthesis [3, 4]. Moreover, *o*-semiquinones are known to possess chelating ability toward metal ions [5–7], which is particularly important for the activation of electron transfer through interaction with cations acting as Lewis acids [5, 8].

Electron paramagnetic resonance (EPR) spectroscopy has established its important position in investigation of semiquinone radicals in laboratory conditions and in their natural surroundings [8–14]. Also, the formation of a complex between diamagnetic metal ions and semiquinone radicals can be efficiently investigated using the EPR techniques since the *g* and *A* tensors are sensitive to the radical–metal ions interaction [5, 6, 15–18].

Recent years have witnessed an increasing interest in the application of theoretical methods to chemical and biochemical systems [19–21]. One of the most significant quantum chemical methods employed in this type of studies are the ones based on density functional theory (DFT) since these methods can be applied to (nearly) real chemical systems. Organic radicals (including semiquinones) have been the subject of successful DFT studies covering diverse environmental factors significantly affecting the radical various properties as well as their EPR tensors (*g* and *A*) [14, 22–46]. However, far too little attention has been paid to the interaction between the radicals and diamagnetic metal ions. Previously, we reported the results of a detailed DFT study of the influence of Mg^{2+} on the *o*-semiquinone ligands in the formed complexes [47]. In the present work, we aimed to characterize theoretically the effects of the Ca^{2+} ion on the electronic structure of the *o*-semiquinone radicals and on the molecular geometries of the resulting complexes, in correlation with both the *g* tensor components and the characteristics of the previously studied Mg^{2+} complexes. In order to make the comparison meaningful, exactly the same theory levels and software versions were used here as

Electronic supplementary material The online version of this article (doi:10.1007/s00214-013-1383-3) contains supplementary material, which is available to authorized users.

M. Witwicki (✉) · J. Jezierska
Faculty of Chemistry, Wroclaw University, 14 F. Joliot-Curie St., 50-283 Wroclaw, Poland
e-mail: maciej.witwicki@chem.uni.wroc.pl

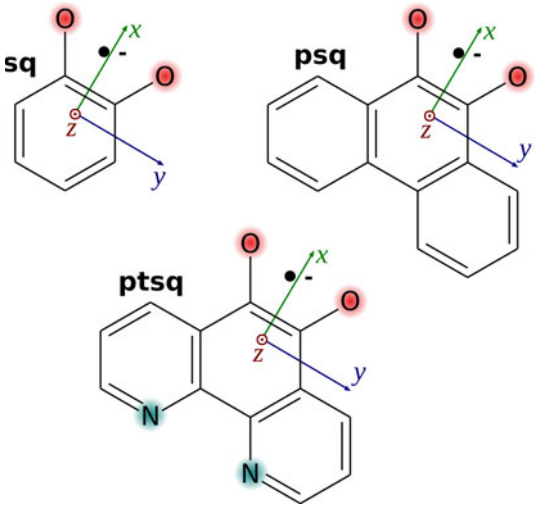

Fig. 1 Schematic structures of anionic semiquinone radical ligands derived from *o*-quinone (**sq**), 9,10-phenanthrenequinone (**psq**), and 1,10-phenanthroline-5,6-dione (**ptsq**). In addition, the principal directions of *g* tensor are shown

before. Moreover, to provide a broader insight into the differences between Mg^{2+} and Ca^{2+} complexes, their relative stability was estimated. This aspect seems to be highly interesting as ubiquinone (Coenzyme Q10) and 2-palmitoylhydroquinone have been shown to transport various metal ions of biological importance ($Mg^{2+}$and Ca^{2+}) [48, 49] or of high toxicity (Sr^{2+} and Ba^{2+}) [50] through membranes. Although the reduced forms of the *p*-quinones correspond directly to the *p*-semiquinones, the mechanisms proposed for Q10 assume its transformation into polyhydroxy forms and the metal ion coordination to the oxygens of the ortho hydroxy groups [49]. Therefore, the theoretical approach to the relative stability of the model complexes with Mg^{2+} and Ca^{2+} ions is expected to reveal which of the ions can be preferred in the transport across membranes.

In this study, semiquinone radicals with different aromaticity, derived from *o*-quinone (**sq**), 9,10-phenanthrenequinone (**psq**), and 1,10-phenanthroline-5,6-dione (**ptsq**) (see Fig. 1), were chosen as the model ligands coordinating Ca^{2+} ions.

2 Computational details

In the calculations, acetonitrile was selected as a solvent because it was mainly used in the experimental studies [5, 8, 51]. Acetonitrile was included in the calculations by using the continuum solvation models (PCM and COSMO), which have been shown to provide an accurate and efficient approximation to the aprotic solvent effects [22, 28, 52, 53].

All the optimizations of molecular structures were carried out using the Gaussian 09 [54] suite of programs employing the popular UB3LYP hybrid functional [55–57] and the TZVP basis set [58]. The initial geometries for the optimizations of the Ca^{2+} complexes with *o*-semiquinone ligands were prepared using the structures determined by X-ray crystallography for similar diamagnetic Ca^{2+} complexes. The coordination number (c.n.) of Ca^{2+} in these diamagnetic systems was found to be predominantly 7 [59, 60] and 8 [61, 62]. In order to make the investigation more complete, also the complexes with c.n. = 6 (octahedral) and c.n. = 4 (square planar and tetrahedral) were included in the computational analysis. To complete the coordination sphere of Ca^{2+}, the optimized structures contained six, five, four or two acetonitrile molecules in addition to the chelating semiquinone ligand. The effect of solvation on geometry was covered by employing the integral equation formalism variant (IEFPCM) of Tomasi's PCM method [63–65]. No symmetry constraints were imposed on the optimization procedures. All the open-shell computations were carried out using the spin-unrestricted formalism. The geometries of the investigated species did not reveal imaginary frequencies. The initial square planar structures underwent convergence to tetrahedral. This result was independent of the *o*-semiquinone ligand and PCM inclusion.

The ORCA electronic structure package [66] was used to calculate the *g* tensors and to perform the Löwdin population analysis. In these undertakings, the hybrid (UB3LYP [55–57] and UPBE0 [67, 68]) and generalized gradient approximations functionals (UBP86 [69, 70], UPBE [68], and UOLYP [55, 71]), together with the TZVP basis set [58] were employed. The conductor-like screening model (COSMO) [72, 73] was the continuum solvation model used in the computations. The *g* tensors were computed using Neese's CPKS method [74] combined with an accurate mean field approximation [RI-SOMF(1X)] [75] to the Breit–Pauli spin–orbit coupling operator [76, 77]. In this work, all the computed components of the *g* tensors are given as *g*-shifts (Δg_{ij}) in parts per million (ppm):

$$\Delta g_{ij} = (g_{ij} - g_e) \times 10^6 \text{ ppm}, \quad (1)$$

where $ij = xx$, yy, zz, and $g_e = 2.002319$ is the free electron *g* value.

In order to examine the relative stability of the radical complexes, Gibbs energies at $T = 298.15$ K were calculated at the (U)B3LYP/TZVP theory level for the process of radical complex ($[ML_{(c.n.-2)}R]^{+\cdot}$) formation from a cation complex with acetonitrile ($[ML_{c.n.}]^{2+}$) and a radical ligand ($R^{-\cdot}$):

$$[ML_{c.n.}]^{2+} + R^{-\cdot} \rightarrow [ML_{(c.n.-2)}R]^{+\cdot} + 2L, \quad (2)$$

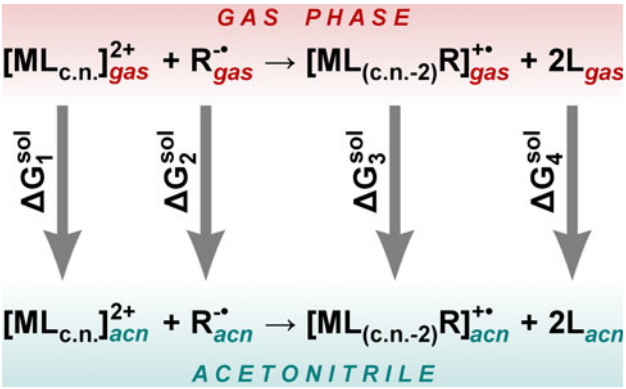

Fig. 2 Thermodynamic cycle used in the calculations of the Gibbs energies for the complexes formation in acetonitrile

where L = CH_3CN, M = Mg or Ca, and $R^{-\cdot}$ = **sq**, **psq** or **ptsq** (all the structures of the Mg^{2+} complexes were taken from our former work [47]). The Gibbs energies were calculated for the reaction taking place in the gas phase (given in Eq. 2) and in acetonitrile using the thermodynamic cycle shown in Fig. 2. The solvation energies were obtained from single-point PCM computations. The structures of the acetonitrile molecules (L) and of the cations coordinated to the acetonitrile molecules for various c.n. ($[ML_{c.n.}]^{2+}$) were optimized as described above, but the restricted formalism (RB3LYP/TZVP) was used for the closed-shell species. The DFT methods have been proved useful in the prediction of the Ca^{2+} and Mg^{2+} affinity for nonradical ligands [78–80].

3 Results and discussion

Figure 3 shows optimized geometries of the Ca^{2+} complexes with **sq**. Similar figures for **psq** and **ptsq** are given in Supplementary Materials (Figure S1). These figures also illustrate the rules used for structure naming: (1) The short names of *o*-semiquinones given in Fig. 1 define the radical molecule; (2) an Arabic numeral following a short name of an *o*-semiquinone indicates the c.n. of Ca^{2+}; and (3) the letter A in the superscript indicates that the continuum solvation model was included in the calculation. The above rules were also applied to the Mg^{2+} complexes taken from our previous work [47], but an asterisk * was used for the latter to distinguish them from the Ca^{2+} complexes.

3.1 Molecular structure and spin density

From the EPR point of view, it is interesting to see how the formation of the Ca^{2+} complex affects the spin density of the semiquinone ligands. The changes are illustrated in this article with the Löwdin spin populations (see Table 1). Since the spin density of semiquinones depends on the length of the bonds between hydroxyl oxygens and carbon atoms ($R_{C–O}$) [14, 22, 34, 52], the impact of Ca^{2+} complexation on $R_{C–O}$ should be first taken under investigation. Regardless of the c.n., the $R_{C–O}$ distances predicted for the Ca^{2+} complex with the *o*-semiquinones are significantly larger than the ones for the uncomplexed radicals, e.g., $R_{C–O}$ increased from 1.265 Å for $\mathbf{sq}^{\mathbf{A}}$ to 1.271 Å for $\mathbf{sq8}^{\mathbf{A}}$. The increase in $R_{C–O}$ was less significant for the complexes with a higher c.n. The $R_{C–O}$ elongation leads to a more profound spin population on the ipso carbons, as compared with the uncomplexed radical. At the same time, the spin population on the hydroxyl oxygen atoms becomes significantly lower. Importantly, the larger $R_{C–O}$ values (and slightly more significant changes in spin populations) were observed in the case of Mg^{2+} coordination [47].

An interesting problem seems to be the concentration of spin density on the Ca atom. In each of the investigated complexes, the spin population on Ca was found to be barely noticeable. To ensure that this is not due to the basis set effect, the computations with other basis sets (SVP, TZVPPP, QZVP) were conducted. Regardless of the basis set used, the spin population remained insignificant (see Table S2 in Supplementary Materials). Thus, Ca^{2+} complexation generates a change of spin populations similar to

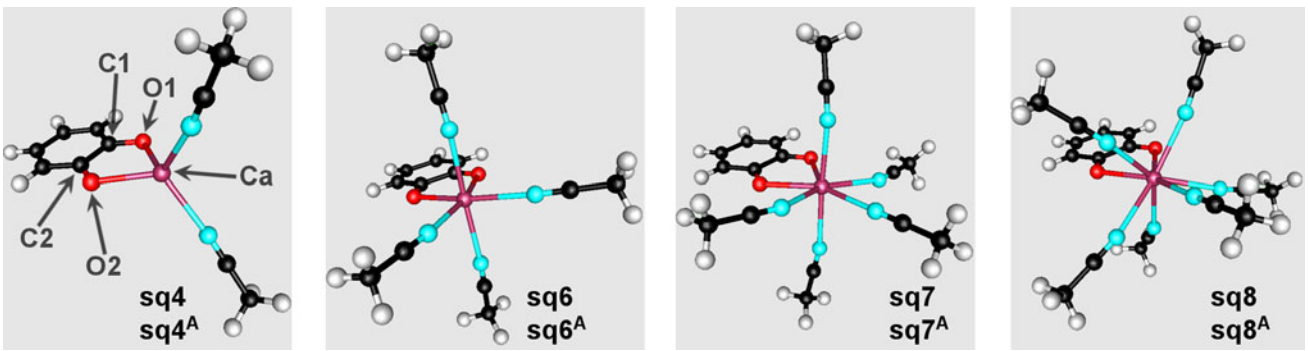

Fig. 3 Optimized structures of the Ca^{2+} complexes with **sq**; the atoms numbering shown for **sq4** is valid for all the structures discussed in the paper

Table 1 Lengths of the C–O and O–M (M = Ca or Mg) bonds (in Å) as well as Löwdin spin populations (ρ); all computed at the UB3LYP/TZVP theory level

	R_{C1-O1}	R_{C2-O2}	R_{O1-M}	R_{O2-M}	ρ_{C1}	ρ_{C2}	ρ_{O1}	ρ_{O2}	ρ_{M}
sq	1.252	1.252	n/a	n/a	0.060	0.060	0.253	0.253	n/a
sq^{A}	1.265	1.265	n/a	n/a	0.104	0.104	0.243	0.243	n/a
Ca^{2+} complexes									
sq4	1.285	1.285	2.320	2.320	0.183	0.183	0.196	0.188	0.008
sq4^{A}	1.274	1.273	2.489	2.486	0.149	0.149	0.212	0.213	0.003
sq6	1.277	1.277	2.381	2.381	0.149	0.149	0.215	0.215	0.003
sq6^{A}	1.273	1.273	2.498	2.496	0.144	0.144	0.217	0.217	0.002
sq7	1.274	1.274	2.441	2.441	0.139	0.139	0.219	0.219	0.003
sq7^{A}	1.271	1.271	2.488	2.487	0.135	0.135	0.222	0.221	0.002
sq8	1.271	1.271	2.465	2.465	0.128	0.129	0.226	0.226	0.000
sq8^{A}	1.271	1.270	2.551	2.551	0.127	0.126	0.228	0.228	0.000
Mg^{2+} complexes									
sq4* [a]	1.291	1.291	1.968	1.968	0.182	0.182	0.188	0.188	0.005
sq4^{A}* [a]	1.288	1.288	2.002	2.002	0.174	0.175	0.194	0.194	0.003
sq6* [a]	1.280	1.280	2.053	2.053	0.152	0.152	0.214	0.214	0.000
sq6^{A}* [a]	1.280	1.280	2.080	2.078	0.151	0.151	0.215	0.215	−0.001

Values for the complexes of **psq** and **ptsq** are given in Supplementary Materials (Table S1)

[a] The values taken from [47]

the one observed by us previously for the Mg^{2+} complexation [47]. The impact of the two cations on spin populations and R_{C-O} is qualitatively similar to the changes induced by the solvent [14, 22, 31, 34, 52], but it is quantitatively far greater.

It is essential to compare the lengths of the metal–oxygen bonds for Ca^{2+} and Mg^{2+} complexes. The R_{O-Ca} values are predicted to increase with the c.n. from 2.489 Å for **sq4^{A}** to 2.498 Å for **sq6^{A}** and to 2.551 Å for **sq8^{A}** (Table 1), similarly to the change in R_{O-Mg} from 2.002 Å for **sq4^{A}*** (tetrahedral) to 2.080 Å for **sq6^{A}*** (octahedral). It is apparent that the R_{O-Ca} values are significantly higher than the R_{O-Mg} values.

3.2 *g* Tensor

It is known that the DFT methods might misestimate the covalent character of metal–ligand bonds [81–83]. Although this is more frequently the case of transition metal coordination compounds, we decided to calculate the Δg tensors with a vast array of functionals (UBP86, UPBE, UOLYP, UB3LYP, UPBE0). The comparison of the *g* tensors presented in Table 2 shows that all the methods, both GGA and hybrid approximations, yield similar outcomes. Therefore, one can expect that the variation of the covalency on the functional is small. The reason for this is the fact that the interaction between the Ca^{2+} ion and the *o*-semiquinones is mainly electrostatic in nature; therefore, a minor contribution of the covalency to the computed Δg tensors is not to be significantly dependent on the functional.

Figure 1 shows principal axes of the *g* tensor whose directions remained unaffected by Ca^{2+} interaction. This result was independent of the examined model complex and the used methodology (various functionals and/or continuum solvent model inclusion).

The Δg_{zz} values were found to be far less sensitive to the complexation (see Table 2) than the perpendicular components (Δg_{xx} and Δg_{yy}). The Δg_{zz} magnitude tends to rise when the radical interacts with the cation. A good example of this is the semiquinone derived from *o*-quinone. Δg_{zz} increases from −125 ppm for **sq^{A}** to −22 ppm for **sq4^{A}**, 11 ppm for **sq6^{A}**, 27 ppm for **sq7^{A}**, and 44 ppm for **sq7^{A}** (employing UB3LYP). It is also clear from this data that Δg_{zz} becomes more positive for the complexes with the larger c.n.

As mentioned above, the spin populations on the hydroxyl oxygens markedly decrease upon the *o*-semiquinone interaction with Ca^{2+}. According to Stone's qualitative model [84, 85], such spin redistribution ought to reduce the Δg_{xx} and Δg_{yy} values. Our DFT predictions of the Δg tensor prove the correctness of this hypothesis. Regardless of the c.n., the lowering of the perpendicular components is substantial. In general, the effects of Ca^{2+} and Mg^{2+} complex formation on the Δg tensor are similar, albeit the interaction between Mg^{2+} and the *o*-semiquinones, as revealed by the shorter O–Mg bonds and ΔG^{298} (to be discussed below), is clearly stronger

Table 2 Δg tensors (in ppm) calculated using the UB3LYP, UBP86, UPBE, UPBE0, and UOLYP functionals

	UB3LYP/TZVP				UBP86/TZVP				UPBE0/TZVP			
	Δg_{xx}	Δg_{yy}	Δg_{zz}	Δg_{iso}	Δg_{xx}	Δg_{yy}	Δg_{zz}	Δg_{iso}	Δg_{xx}	Δg_{yy}	Δg_{zz}	Δg_{iso}
Ca^{2+} complexes												
sq4	3610	2249	−24	1945	3620	2455	−15	2020	3591	2480	−12	2020
sq4^{A}	3878	2733	−22	2196	3883	2553	−25	2137	3888	2762	−19	2211
psq4	2903	2215	−75	1681	2784	1993	−79	1566	2897	2249	−72	1691
psq4^{A}	3345	2529	−87	1929	3227	2305	−82	1817	3369	2569	−85	1951
ptsq4	2930	2257	−89	1699	2860	2064	−93	1610	2904	2250	−89	1688
ptsq4^{A}	3436	2621	−102	1985	3344	2403	−99	1883	3444	2634	−101	1992
sq6	4139	2811	9	2320	4071	2583	−4	2216	4116	2821	14	2317
sq6^{A}	4077	2911	11	2333	4052	2718	7	2259	4082	2927	15	2341
psq6	3474	2554	−70	1986	3294	2291	−78	1836	3463	2573	−66	1990
psq6^{A}	3561	2660	−69	2050	3405	2421	−66	1920	3577	2685	−67	2065
ptsq6	3489	2570	−83	1992	3352	2333	−90	1865	3462	2553	−80	1978
ptsq6^{A}	3622	2720	−84	2086	3495	2489	−83	1967	3624	2718	−84	2086
sq7	4276	2884	21	2394	4190	2645	12	2282	4264	2896	25	2395
sq7^{A}	4220	2968	27	2405	4167	2754	24	2315	4228	2982	31	2414
psq7	3564	2584	−60	2030	3356	2309	−54	1870	3569	2606	−56	2039
psq7^{A}	3744	2681	−56	2123	3547	2430	−50	1976	3767	2709	−54	2141
ptsq7	3583	2591	−73	2034	3418	2340	−70	1896	3571	2579	−73	2026
ptsq7^{A}	3835	2758	−71	2174	3665	2507	−67	2035	3846	2759	−71	2178
sq8	4461	3072	28	2520	4333	2821	20	2391	4486	3053	46	2528
sq8^{A}	4378	3134	44	2519	4296	2919	41	2419	4377	3136	34	2516
psq8	3863	2926	−53	2245	3615	2632	−61	2062	3866	2934	−48	2250
psq8^{A}	3881	2924	−48	2252	3662	2656	−48	2090	3900	2938	−45	2264
ptsq8	3860	2922	−68	2238	3651	2647	−78	2073	3848	2897	−64	2227
ptsq8^{A}	3949	2992	−62	2293	3753	2724	−63	2138	3955	2980	−59	2292
Exptl for Ca^{2+} complexes with												
sq in water[a]				1981				1981				1981
psq in acetonitrile[b]				1681				1681				1681
ptsq in acetonitrile[b]				2281				2281				2281
PQQ in acetonitrile[c]	3531	2861	−199	2064	3531	2861	−199	2064	3531	2861	−199	2064
o-Semiquinones												
sq	5179	4406	−111	3158	4903	4216	−105	3005	5257	4465	−112	3203
sq^{A}	4789	3989	−125	2884	4696	3794	−118	2791	4846	4043	−127	2921
psq	4571	4163	−89	2882	4140	3781	−79	2614	4652	4262	−90	2941
psq^{A}	4295	3841	−94	2681	4041	3513	−84	2490	4352	3935	−96	2730
ptsq	4584	4302	−95	2930	4192	3947	−87	2684	4645	4377	−96	2975
ptsq^{A}	4328	3965	−99	2731	4103	3658	−90	2557	4372	4035	−101	2769
Exptl for												
sq in water[a]				2281				2281				2281
psq in acetonitrile[b]				2481				2481				2481
ptsq in acetonitrile[b]				2681				2681				2681

	UPBE/TZVP				UOLYP/TZVP			
	Δg_{xx}	Δg_{yy}	Δg_{zz}	Δg_{iso}	Δg_{xx}	Δg_{yy}	Δg_{zz}	Δg_{iso}
Ca^{2+} complexes								
sq4	3669	2260	−20	1970	3624	2287	−11	1967
sq4^{A}	3946	2564	−23	2162	3882	2572	−15	2147

Table 2 continued

	UPBE/TZVP				UOLYP/TZVP			
	Δg_{xx}	Δg_{yy}	Δg_{zz}	Δg_{iso}	Δg_{xx}	Δg_{yy}	Δg_{zz}	Δg_{iso}
psq4	2849	1999	−74	1591	2896	2013	−73	1612
psq4^{A}	3296	2317	−78	1845	3322	2330	−79	1858
ptsq4	2926	2084	−86	1641	2951	2116	−87	1660
ptsq4^{A}	3412	2426	−93	1915	3421	2454	−96	1926
sq6	4145	2610	−2	2251	4081	2637	8	2242
sq6^{A}	4135	2747	9	2297	4081	2766	17	2288
psq6	3377	2315	−75	1872	3412	2341	−75	1893
psq6^{A}	3491	2447	−64	1958	3528	2468	−65	1977
ptsq6	3436	2369	−86	1906	3450	2412	−87	1925
ptsq6^{A}	3580	2526	−79	2009	3598	2564	−82	2027
sq7	4262	2673	13	2316	4207	2702	23	2310
sq7^{A}	4249	2786	26	2353	4207	2808	33	2349
psq7	3436	2328	−53	1904	3479	2357	−54	1927
psq7^{A}	3632	2450	−48	2011	3674	2473	−51	2032
ptsq7	3497	2372	−68	1934	3520	2422	−71	1957
ptsq7^{A}	3748	2541	−65	2075	3772	2583	−70	2095
sq8	4436	2840	31	2436	4361	2852	41	2418
sq8^{A}	4347	2928	27	2434	4294	2931	35	2420
psq8	3699	2662	−60	2100	3695	2662	−57	2100
psq8^{A}	3748	2688	−46	2130	3756	2695	−45	2135
ptsq8	3733	2688	−75	2115	3715	2703	−73	2115
ptsq8^{A}	3836	2768	−60	2181	3829	2787	−61	2185
Exptl for Ca^{2+} complexes with								
sq in water[a]				1981				1981
psq in acetonitrile[b]				1681				1681
ptsq in acetonitrile[b]				2281				2281
PQQ in acetonitrile[c]	3531	2861	−199	2064	3531	2861	−199	2064
o-Semiquinones								
sq	4978	4277	−102	3051	4852	4190	−96	2982
sq^{A}	4794	3850	−115	2843	4686	3797	−113	2790
psq	4210	3814	−75	2650	4191	3742	−80	2618
psq^{A}	4139	3558	−78	2540	4146	3528	−86	2530
ptsq	4262	3987	−82	2722	4230	3906	−87	2683
ptsq^{A}	4197	3706	−85	2606	4179	3664	−90	2584
Exptl for								
sq in water[a]				2281				2281
psq in acetonitrile[b]				2481				2481
ptsq in acetonitrile[b]				2681				2681

[a] Eaton [16], experimental values obtained in water; therefore, for the **sq** free radical, somewhat more significant overestimation of calculated Δg_{iso} is observed; see e.g. [14, 22, 31, 34, 52] for investigation of the hydrogen bonds effect

[b] Yuasa et al. [5]

[c] Pyrroloquinoline quinone (2,7,9-tricarboxypyrroloquinoline), values taken from [11]

compared to Ca^{2+}. The stronger interaction in the case of Mg^{2+} should be expected to induced more significant decrease of Δg_{xx} and Δg_{yy}. This, however, was not observed, suggesting that the g factor is not a sufficient criterion for the strength of the interaction between an *o*-semiquinone and metal cation.

Interestingly, the COSMO correction decreases Δg-shifts for the solvated semiquinone, as expected [14, 22,

34, 52], but increases them for the complexed semiquinone. The complex can be considered as comprising of two parts: the semiquinone ligand and the cation with acetonitrile molecules. The COSMO correction stabilizes the latter part of the complex, decreasing the strength of the cation–semiquinone interaction and therefore decreasing the cation effect on the Δg tensor. The weakening of Ca^{2+}–semiquinone interaction is clearly seen in the COSMO-induced R_{Ca-O} elongation.

Unfortunately, a direct comparison of the calculated Δg tensor diagonal components with their experimental counterparts is limited as very few high-field experiments have been performed so far. Therefore, we focused on the values of the Δg_{iso} parameters. Since the calculated Δg_{iso} values for all the considered models are close to the experimental ones, it is impossible to determine explicitly on the basis of Δg_{iso} which coordination sphere is preferred in real chemical systems. To answer this question, the Gibbs free energies were calculated for the reaction given in Eq. 2; the results are presented below. On the other hand, a general agreement between the calculated Δg tensor components and ones experimentally determined for similar systems was expected to be a good additional way of verifying the quality of the computations. The choice of pyrroloquinoline quinone (2,7,9-tricarboxypyrroloquinoline, PQQ), a quinone cofactor belonging to a class of dehydrogenases known as quinoproteins, seems to be the most appropriate. PQQ is bonded to the Ca^{2+} ion and exhibits an EPR spectrum with the $\Delta g_{xx} = 3{,}531$, $\Delta g_{yy} = 2{,}861$, and $\Delta g_{zz} = -199$ components [10, 11]. The magnitude of the Δg-shifts predicted by us for the model *o*-semiquinone complexes is similar, despite the chemical differences. This fact (in combination with the good agreement between experimental and theoretical Δg_{iso}) suggests the high accuracy of the computations.

The distribution of spin density in the *o*-semiquinones coordinating Ca^{2+} (and Mg^{2+}) gives rise to an interesting question about the direct contribution of the Ca^{2+} (and Mg^{2+}) ion to the perpendicular Δg tensor components. Minor spin populations on the metal cations to a certain degree suggest that such a direct impact should be insignificant and only strong indirect effects may be expected. To investigate this problem, we performed a theoretical analysis of the atomic contributions to Δg_{xx} and Δg_{yy}. In order to make this analysis complete, the calculations were also done (for the first time) for the representative Mg^{2+} complex investigated by us previously [47].

In one-component DFT calculations, the total Δg tensor is given as a sum of three contributions [74, 86, 87]:

$$\Delta g_{st} = \delta_{st}\Delta g^{RMC} + \Delta g_{st}^{DC} + \Delta g_{st}^{PSO}, \quad (3)$$

where Δg^{RMC} is the relativistic mass correction to kinetic energy, δ_{st} is the Kronecker delta function ensuring that Δg^{RMC} contributes only to the diagonal components of the Δg tensor ($s = t$), Δg_{st}^{DC} is the diamagnetic correction and Δg_{st}^{PSO}, is the paramagnetic spin–orbit term. The values of the three terms are given in Table 3.

Irrespective of the interactions with the metal ion, the predicted Δg^{RMC} and Δg_{st}^{DC} values were found to be of minor magnitude. Moreover, their opposite signs lead to the mutual cancelation of the two terms whereby the Δg_{xx} and Δg_{yy} components are dominated by Δg_{st}^{PSO}. In this case, an accurate approximation of the atomic contributions to the Δg tensor can be obtained via the breakdown of Δg_{st}^{PSO} into the contributions from the particular atoms. Since the mean field approximation to the molecular spin–orbit coupling operator employed in this work [RI-SOMF(1X)] [75] takes into account the mulicenter terms (except for the exchange part), these terms have to be neglected to obtain the atomic contributions. Considering that such an omission may cause significant errors [75], in Table 3, the Δg_{st}^{PSO}(1c) values calculated in the one-center approximation are compared with the ones calculated including the multicenter terms (Δg_{st}^{PSO}), revealing only a limited deviation.

The contributions from all the atoms for **sq** were calculated at the UB3LYP/TZVP theory level and are shown in Fig. 4. Both perpendicular components are dominated by the contributions from the oxygens. This is in agreement with the previous reports for *p*-semiquinone [34] and the phenoxyl radical [35]. The contributions from carbon atoms, even from these in the ipso positions, are considerably small. Moreover, the contributions from the different carbons to Δg_{xx} have opposite signs, which leads to their mutual cancelation.

The inclusion of the COSMO model ($\mathbf{sq^A}$) results in a significant decrease in the contributions from the oxygens to the Δg_{xx} and Δg_{yy} components (see Table 3). After the attachment of Mg^{2+} or Ca^{2+} to **sq**, barely noticeable contributions of the metal atoms were predicted. Thus, the observed diminution of Δg_{xx} and Δg_{yy} upon the complex formation is exclusively the result of the reduced contributions from the oxygens. Consequently, the impact of a diamagnetic metal ion on the Δg tensor of the semiquinone radical can be described as indirect; a metal ion does not bring any significant direct contribution, but causes a decrease in the contributions from hydroxyl oxygen atoms.

Table 3 is quite informative in another way. As it was mentioned above, Δg_{zz} increases on complex formation, and this table shows that this increase is related primarily to the rise of Δg_{zz}^{DC} and secondarily to the growth of Δg_{zz}^{PSO} term.

As it was demonstrated in our former systematic study of Mg^{2+} complexes with *o*-semiquinone ligands [47], breaking down of the dominant Δg_{st}^{PSO} term into the

Table 3 Individual contributions to the Δg tensor components and the direct contributions of selected atoms obtained employing the one-center approximation

	Radical						Ca^{2+} complex			Mg^{2+} complex		
	sq			**sq^{A}**			**sq6^{A}**			**sq6^{A}***		
	Δg_{xx}	Δg_{yy}	Δg_{zz}	Δg_{xx}	Δg_{yy}	Δg_{zz}	Δg_{xx}	Δg_{yy}	Δg_{zz}	Δg_{xx}	Δg_{yy}	Δg_{zz}
Δg^{total}	5179	4406	−111	4789	3989	−125	4077	2911	11	4045	2806	−46
Δg^{RMC}	−231	−231	−231	−229	−229	−229	−223	−223	−223	−225	−225	−225
Δg^{DC}	154	177	142	149	178	136	169	249	223	164	226	197
Δg^{PSO}	5256	4460	−22	4869	4040	−32	4131	2885	11	4106	2805	−18
Δg^{PSO}(1c)	5145	4412	−24	4832	3920	−33	4176	2822	0	4098	2701	−29
$\Delta g^{\text{PSO}} - \Delta g^{\text{PSO}}$(1c)	112	48	2	37	120	1	−45	63	11	8	104	11
Selected atoms contributions to Δg(1c)												
O1	2640	2098	−14	2495	1831	−17	2171	1397	2	2138	1255	0
O2	2639	2099	−14	2495	1831	−17	2171	1397	2	2143	1257	0
C1	−137	40	1	−133	60	0	−107	46	−9	−119	56	−8
C2	−137	40	1	−133	60	0	−107	46	−9	−119	56	−8
Ca or Mg	n/a	n/a	n/a	n/a	n/a	n/a	−32	−132	26	−22	−39	9

All calculated at the UB3LYP/TZVP theory level and given in ppm

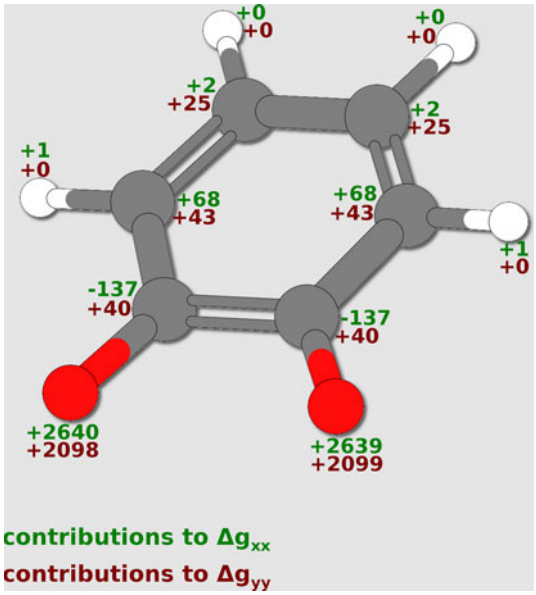

Fig. 4 Contributions of the particular atoms to Δg_{xx} (*green*) and Δg_{yy} (*maroon*) for **sq**; calculated at the UB3LYP/TZVP theory level

contributions originating from the particular excited states can be fruitful for the understanding of the Δg tensor changes on metal ions complexation. To provide similar insight in this work, the alternative one-component method proposed by Schreckenbach and Ziegler [86], as implemented in the ADF package [88], was used. In this method [86]:

$$\Delta g_{st}^{\text{PSO}} = \sigma_{st} + \Delta g_{st}^{\text{PSO,occ-occ}} + \Delta g_{st}^{\text{PSO,occ-vir}}, \tag{4a}$$

$$\sigma_{st} = \frac{1}{2c}\sum_{\gamma=\alpha,\beta} 2m_\gamma \sum_{i=1}^{n_\gamma} n_i^\gamma \sum_{\lambda,\nu}^{2\text{M}} d_{\lambda i} d_{\nu i} \left\langle \chi_\lambda \middle| \left(\overrightarrow{R_\lambda}\, \overrightarrow{R_\nu} \right)_s h_t^{01} \middle| \chi_\nu \right\rangle, \tag{4b}$$

$$\Delta g_{st}^{\text{PSO,occ-occ}} = \sum_{\gamma=\alpha,\beta} 2m_\gamma \sum_{i,j=1}^{n_\gamma} n_i^\gamma S_{ij}^{1,s} \langle \Psi_i | h_t^{01} | \Psi_j \rangle, \tag{4c}$$

$$\Delta g_{st}^{\text{PSO,occ-vir}} = 2\sum_{\gamma=\alpha,\beta} 2m_\gamma \sum_{i=1}^{n_\gamma} n_i^\gamma \sum_{a}^{\text{vir}} u_{aj}^{1,s} \langle \Psi_i | h_t^{01} | \Psi_a \rangle. \tag{4d}$$

The term σ_{st} has been shown to be numerically irrelevant [86, 89], and it is therefore neglected in the further discussion; $\Delta g_{st}^{\text{PSO,occ-occ}}$ are the couplings between occupied orbitals and $\Delta g_{st}^{\text{PSO,occ-vir}}$ between occupied and virtual ones; h_t^{01} is the paramagnetic spin–orbit operator defined in [86]; Ψ_i and Ψ_a are occupied and virtual Kohn–Sham orbitals, respectively; the orbitals are expanded into the set of 2M basis functions $\{\chi_\lambda\}$; the expansion coefficients are the $d_{\lambda i}$; n_i^γ is the occupation number of Ψ_i; $S_{ij}^{1,s}$ and $u_{aj}^{1,s}$ are the first-order occupied–occupied and occupied–virtual coefficients, respectively; and the coefficients $2m_\gamma$ afford the correct signs for α and β spins ($m_\alpha = ½$ and $m_\beta = -½$). All the Δg tensor calculations performed with the ADF package were spin-unrestricted, based on the scalar Pauli Hamiltonian and employing the UBP86 functional in concert with the standard all-electron Slater-type TZP basis set. The ADF program was used because the implementation included in it allows to analyze $\Delta g_{st}^{\text{PSO,occ-vir}}$ in terms of single excitations.

The $\Delta g_{st}^{\mathrm{PSO,occ-vir}}$ term is usually the most important one [89], and it is shown here to dominate the perpendicular components of the uncomplexed **sq** radical and the studied complexes (see Table 4). Δg_{zz} is very small in magnitude because of the insignificant coupling between occupied and virtual orbitals. Nonetheless, $\Delta g_{zz}^{\mathrm{PSO,occ-vir}}$ is slightly increased after the Ca^{2+} or Mg^{2+} complex formation. To meaningfully discuss the contribution of excited states to the Δg_{xx} and Δg_{yy} components, the possible excitations were classified into three groups: (1) from the doubly occupied orbitals to the SOMO (D → S); (2) from the SOMO to the virtual ones (S → V); and (3) from the doubly occupied orbitals to the virtual (D → V). The last group is expected to bring small contributions to the Δg tensor of organic radicals as contributions of these excited states arise from the spin polarization solely. The contributions of the three groups of excited states to $\Delta g_{st}^{\mathrm{PSO,occ-vir}}$ are listed in Table 4 and visualized in Fig. 5.

The perpendicular components for **sq** are dominated by the contributions from D → S excited states, in accordance with the report for *p*-semiquinone [52]. This group of excited states is the preeminent one also after the Ca^{2+} and Mg^{2+} complexation; however, its contribution is significantly decreased. For the *o*-semiquinone radical anion **sq**, Δg_{xx} and Δg_{yy} components are mainly prevailed by the contributions from HOMO-2 → SOMO and HOMO → SOMO excited states, respectively (the both excited states are of the D → S type). The formation of a complex between Ca^{2+} and **sq** results in the significantly reduced contributions of these two excited states, and consequently, Δg_{xx} and Δg_{yy} decrease on the complex formation. Interestingly, after the complex formation, the HOMO → SOMO contribution becomes nearly negligible. The isosurfaces of SOMO, HOMO, and HOMO-2 are shown in Fig. 5c.

3.3 Relative stability

It would be interesting to find which metal cation, Mg^{2+} or Ca^{2+}, forms more stable complexes with *o*-semiquinone ligands. The enthalpies $\left(\Delta H_{\mathrm{gas}}^{298}\right)$, the entropies $\left(\Delta S_{\mathrm{gas}}^{298}\right)$, the Gibbs energies in the gas phase and in acetonitrile ($\Delta G_{\mathrm{gas}}^{298}$ and ΔG^{298}, respectively) and the changes in the solvation energies $\left(\sum \Delta G_{\mathrm{sol}}^{298}\right)$ calculated for the radical complexes formation (Eq. 2) are reported in Table 5.

First, it is sensible to compare the Gibbs energies calculated for the complex formation taking place in acetonitrile (ΔG^{298}) and in the gas phase ($\Delta G_{\mathrm{gas}}^{298}$). The $\Delta G_{\mathrm{gas}}^{298}$ values are significantly more negative, whereby the formation of the semiquinone complex with Mg^{2+} or Ca^{2+} from the free anionic radical and cation complexed by acetonitrile molecules tends to be energetically more beneficial in the gas phase. This can be explained by the fact that the stability of ions is increased by solvation more significantly than the stability of uncharged molecules. Considering that the complex formation in Eq. 2 is inseparable from the reduction of the charge (one 2+ cation and one 1− radical anion are the substrates and one 1+ radical complex is the product), the solvation of the substrates is expected to be energetically more beneficial than the solvation of the products, which should lead to the lowering of the radical binding affinity in the solution. This presumption is clearly corroborated by the positive change of solvation energy $\sum \Delta G_{\mathrm{sol}}^{298}$ (see Table 5). Despite the positive $\sum \Delta G_{\mathrm{sol}}^{298}$ values, the resulting ΔG^{298} is predicted to stay negative.

Table 4 Contributions of excited states to the *g* tensor; all calculated at the UBP86/TZP theory level with the ADF package employing the method proposed by Schreckenbach and Ziegler [86]

	Radical			Ca^{2+} complex			Mg^{2+} complex		
	sq			**sq6**			**sq6***		
	Δg_{xx}	Δg_{yy}	Δg_{zz}	Δg_{xx}	Δg_{yy}	Δg_{zz}	Δg_{xx}	Δg_{yy}	Δg_{zz}
$\Delta g^{\mathrm{total}}$	6032	5116	−212	4278	2931	−339	4692	3175	−268
Δg^{RMC}	−216	−216	−216	−208	−208	−208	−212	−212	−212
Δg^{DC}	82	67	41	80	66	28	80	65	42
Δg^{PSO}	6166	5265	−37	4405	3073	−159	4824	3322	−98
$\Delta g^{\mathrm{PSO,occ-occ}}$	258	584	−17	281	556	30	320	599	20
$\Delta g^{\mathrm{PSO,occ-vir}}$									
Total	5908	4681	−20	4124	2517	−189	4504	2723	−118
$\sum$(D → V)	−178	37	−20	−206	177	19	−330	−69	−32
$\sum$(S → V)	−108	174	0	−168	−168	64	−169	168	−68
$\sum$(D → S)	6194	4469	0	4498	2509	−272	5003	2624	−18
HOMO → SOMO	0	2016	0	0	295	0	0	303	0
HOMO-2 → SOMO	4980	0	0	3749	0	0	4228	0	0

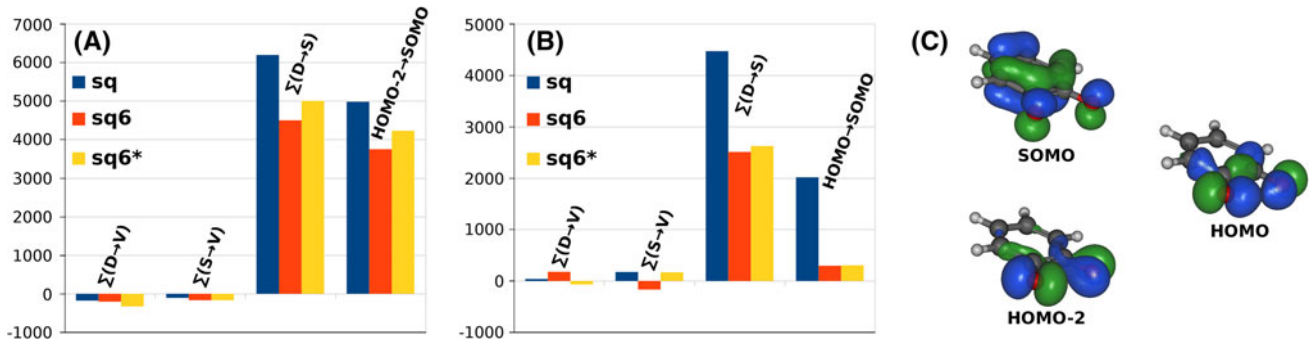

Fig. 5 Graphical illustration of various excited states contributions to Δg_{xx} (**a**) and to Δg_{yy} (**b**). In addition, molecular orbitals connected to the excited states giving significant contributions to the Δg tensor are shown (**c**). Labels to the orbitals were given according to the results for **sq**

Table 5 Selected thermodynamic properties calculated at the (U)B3LYP/TZVP theory level according to the thermodynamic cycle shown in Fig. 2

	ΔH^{298}_{gas} (kcal mol^{-1})	ΔS^{298}_{gas} [cal (mol K)$^{-1}$]	ΔG^{298}_{gas} (kcal mol^{-1})[a]	$\sum \Delta G^{298}_{sol}$ (kcal mol^{-1})[b]	ΔG^{298} (kcal mol^{-1})[c]
Ca^{2+} complexes					
sq4	−144.1	21.0	−150.4	131.1	−19.3
psq4	−143.2	11.8	−146.7	128.0	−18.7
ptsq4	−135.2	10.8	−138.4	122.1	−16.4
sq6	−130.1	57.9	−147.4	118.8	−28.6
psq6	−126.2	58.5	−143.6	114.8	−28.8
ptsq6	−119.5	57.8	−136.8	110.0	−26.7
sq7	−129.1	49.1	−143.7	117.2	−26.5
psq7	−124.8	45.5	−138.3	112.3	−26.1
ptsq7	−118.2	45.0	−131.6	107.1	−24.5
sq8	−125.5	34.5	−135.8	113.0	−22.9
psq8	−120.4	42.1	−133.0	109.6	−23.3
ptsq8	−114.4	42.3	−127.1	104.3	−22.7
Mg^{2+} complexes					
sq4*	−154.2	38.5	−165.6	135.5	−30.2
psq4*	−152.4	38.8	−163.9	126.9	−37.0
ptsq4*	−143.1	36.8	−154.1	133.6	−20.5
sq6*	−140.3	33.2	−150.2	123.4	−26.8
psq6*	−136.8	32.8	−146.6	114.1	−32.5
ptsq6*	−129.7	31.5	−139.1	120.2	−18.9

The asterisks (*) indicate the Mg^{2+} complexes (structures taken from Ref. [47])

[a] $\Delta G^{298}_{gas} = \Delta H^{298}_{gas} - T\Delta S^{298}_{gas} = \Delta H^{298}_{gas} - 298.15\Delta S^{298}_{gas}$

[b] $\sum \Delta G^{298}_{sol} = \Delta G^{sol}_3 + 2\Delta G^{sol}_4 - \Delta G^{sol}_1 - \Delta G^{sol}_2$; ΔG^{sol}_i are defined in Fig. 2 and were obtained from the single-point PCM calculations

[c] $\Delta G^{298} = \Delta G^{298}_{gas} + \sum \Delta G^{298}_{sol}$

For the Ca^{2+} complexes, the most negative ΔG^{298} values were obtained for c.n. = 6, strongly suggesting the formation of the complexes with this c.n. in real chemical systems. On the other hand, for c.n. = 4, the ΔG^{298} values are the least negative, indicting a low probability of such Ca^{2+} complex formation. In contrast, for the Mg^{2+} ion, c.n. = 4 is shown to be energetically more profitable as the predicted ΔG^{298} values are considerably lower than for the complexes with c.n. = 6. To understand why the higher c.n. are energetically beneficial in the case of Ca^{2+} ions, one has to compare the ion radius of the both cations. Ca^{2+} has significantly greater radius (1.00 Å) [90] than the Mg^{2+} (0.72 Å) [90]; in consequence, Ca^{2+} may be surrounded by a larger number of ligands without significant steric repulsion between them.

Another point of concern is the relative stability of the complexes containing various *o*-semiquinone ligands. In

general, the relative stabilities of Ca^{2+} coordination compounds with **sq** and **psq** radical ligands are comparable; however, in the case of Mg^{2+}, the stability of the **psq** complexes, clearly indicated by the more negative ΔG^{298} value, is noticeably increased as compared with **sq**. The coordination of both cations to the **ptsq** ligand results in lower stability than the coordination to **sq** and **psq**. This can be explained by the fact that the interaction between *o*-semiquinone radicals and Mg^{2+} and Ca^{2+} cations is mainly electrostatic in nature, whereby the stability of the formed complexes decreases as the negative charge located on the hydroxyl oxygens atoms is reduced. In the case of **ptsq**, the negative charge on the O atoms should be moderately diminished as compared with **sq** and **psq**, since the **ptsq** molecule contains two N atoms that are additional attractors of the negative charge. This can be illustrated using the Löwdin atomic charges. For the hydroxyl oxygens of **sq** and **psq**, they are predicted to be −0.32 and −0.31, respectively, while for **ptsq**, just −0.27.

Perhaps the most interesting is the relative stability of the Ca^{2+} and Mg^{2+} complexes with *o*-semiquinones since the two cations usually coexist in natural systems and so competition between them is expected to occur. As it can be seen in Table 5, the most negative ΔG^{298} values are predicted for Mg^{2+} complexes with c.n. = 4. This fact strongly suggests that the formation of the *o*-semiquinone complexes with this cation is more favorable, and therefore, Mg^{2+} can be expected as preferred over Ca^{2+} in the mechanism of cation transport through membranes [49].

In our opinion, it is always sensible to confront theoretical results with more general ideas, here with the Pearson hard and soft acids and bases concept (HSAB) [91]. According to HSAB, certain metal ions (hard Lewis acids) exhibit high affinity for oxygen donor ligands. Thus, the harder the Lewis acid, the stronger the preference for O donors. For the complexes of Mg^{2+} and Ca^{2+} with *o*-semiquinones, the $Mg^{2+} > Ca^{2+}$ stability order is expected as Mg^{2+} is considered to be a moderately harder acid than Ca^{2+} due to the same +2 charge but noticeably smaller size. To summarize, in spite of its limitations, HSAB gives a qualitative answer being in agreement with the results yielded by DFT methods.

4 Conclusions

This paper has provided a detailed insight into the interaction between *o*-semiquinone radicals and Ca^{2+} ions. Good agreement between the calculated and experimental g_{iso} parameters, supported by accordance of the calculated *g* tensors with the experimental data for PQQ, suggests that DFT methods are suitable not only for theoretical examination of this parameter but also may provide insight into the molecular and electronic structure of the radical species interacting with diamagnetic metal ions. In other words, this good agreement between the theoretical and experimental Δg_{iso} values might be treated as an indication that the other predicted properties (spin distribution, structural parameters as R_{C-O}, R_{Ca-O}) properly characterize the real systems.

The conducted computations revealed that, in general, the effects of Ca^{2+} and Mg^{2+} complex formation on the Δg tensor are similar, although the interaction between Mg^{2+} and the *o*-semiquinones, as revealed by the shorter O–Mg bonds and more negative ΔG^{298}, is clearly stronger compared to Ca^{2+}. The stronger interaction in case of Mg^{2+} should be expected to induce more significant decrease of Δg_{xx} and Δg_{yy}, but this was not observed. Therefore, this study have shown that the *g* factor is not a reliable criterion for the strength of the interaction between an *o*-semiquinone and diamagnetic metal cation.

The calculated atomic contributions to the Δg tensor indicate that the impact of the metal ion (Ca^{2+} or Mg^{2+}) on the Δg tensor of *o*-semiquinone radicals is mainly indirect. Although the metal ion brings only a barely noticeable direct contribution, it causes a significant decrease in the contributions of hydroxyl oxygens to the Δg_{xx} and Δg_{yy} components. In addition, the contributions of various excited states to the Δg tensor were analyzed. It was shown that the decrease of Δg_{xx} and Δg_{yy} on the complex formation is the consequence of reduced contributions of HOMO-2 → SOMO and HOMO → SOMO excited states.

Another important observation is that the general stability of the Mg^{2+} complexes is higher than that of the complexes with Ca^{2+}. Therefore, in the transport mechanism through membranes with Q10 playing the role of the transfer agent [49], Mg^{2+} ions can be expected to be favored over Ca^{2+}.

Acknowledgments This work was financed from the National Science Centre (NCN) funds allocated on the basis of decision DEC-2011/03/B/ST5/01742. The computations were performed using the computers belonging to the Wrocław Center for Networking and Supercomputing (Grant No. 47).

References

1. Bauld NL (1997) Radicals, ion radicals, and triplets. Wiley-VCH, Weinheim
2. Todres ZV (2003) Organic ion radicals: chemistry and applications. Marcel Dekker, New York
3. Ohashi S, Iemura T, Okada N, Itoh S, Furukawa H, Okuda M, Ohnishi-Kameyama M, Ogawa T, Miyashita H, Watanabe T, Itoh

S, Oh-oka H, Inoue K, Kobayashi M (2010) Photosynth Res 104:305
4. Barber J (2009) Chem Soc Rev 38:185
5. Yuasa J, Suenobu T, Fukuzumi S (2006) ChemPhysChem 7:942
6. Ueda A, Ogasawara K, Nishida S, Ise T, Yoshino T, Nakazawa S, Sato K, Takui T, Nakasuji K, Morita Y (2010) Angew Chem Int Ed 49:6333
7. Vostrikova KE (2008) Coord Chem Rev 252:1409
8. Fukuzumi S, Ohkuboa F, Morimoto Y (2012) Phys Chem Chem Phys 14:8472
9. Zech SG, Hofbauer W, Kamlowski A, Fromme P, Stehlik D, Lubitz W, Bittl R (2000) J Phys Chem B 104:9728
10. Kay CWM, Mennenga B, Görisch H, Bittl R (2004) FEBS Lett 564:69
11. Kay CWM, Mennenga B, Görisch H, Bittl R (2005) J Am Chem Soc 127:7974
12. Jezierski A, Czechowski F, Jerzykiewicz M, Chen Y, Drozd J (2000) Spectrochim Acta A 56:379
13. Jezierski A, Czechowski F, Jerzykiewicz M, Golonka I, Drozd J, Bylinska E, Chen Y, Seaward MRD (2002) Spectrochim Acta A 58:1293
14. Witwicki M, Jezierska J, Ozarowski A (2009) Chem Phys Lett 473:160
15. Witwicki M, Jerzykiewicz M, Jaszewski AR, Jezierska J, Ozarowski A (2009) J Phys Chem A 113:14115
16. Eaton DR (1964) Inorg Chem 3:1268
17. Jerzykiewicz M (2012) Spectrochim Acta A 96:127
18. Jerzykiewicz M (2013) Chemosphere 92:445
19. Kukushkin AK, Jalkanen KJ (2010) Theor Chem Acc 125:121
20. Sinnecker S, Neese F (2007) Top Curr Chem 268:47
21. Alberto ME, Marino T, Russo N, Sicilia E, Toscano M (2012) Phys Chem Chem Phys 14:14943
22. Witwicki M, Jezierska J (2010) Chem Phys Lett 493:364
23. Leopoldini M, Marino T, Russo N, Toscano M (2004) Theor Chem Acc 111:210
24. Geldof D, Krishtal A, Blockhuys F, Van Alsenoy C (2012) Theor Chem Acc 131:1243
25. De Vleeschouwer F, Geerlings P, De Proft F (2012) Theor Chem Acc 131:1245
26. Villamena FA, Locigno EJ, Rockenbauer A, Hadad CM, Zweier JL (2006) J Phys Chem A 110:13253
27. Villamena FA, Locigno EJ, Rockenbauer A, Hadad CM, Zweier JL (2007) J Phys Chem A 111:384
28. Rinkevicius Z, Telyatnyk L, Vahtras O (2004) J Chem Phys 121:5051
29. Rinkevicius Z, Murugan NA, Kongsted J, Aidas K, Steindal AH, Ågren H (2011) J Phys Chem B 115:4350
30. Li X, Rinkevicius Z, Kongsted J, Murugan NA, Ågren H (2012) J Chem Theory Comput 8:4766
31. Mattar SM (2004) J Phys Chem B 108:9449
32. Asher JR, Kaupp M (2008) Theor Chem Acc 119:477
33. Asher JR, Doltsinis NL, Kaupp M (2004) J Am Chem Soc 126:9854
34. Kaupp M, Remenyi C, Vaara J, Malkina OL, Malkin VG (2002) J Am Chem Soc 124:2709
35. Malkina OL, Vaara J, Schimmelpfennig B, Munzarova M, Malkin VG, Kaupp M (2000) J Am Chem Soc 122:9206
36. O'Malley PJ (1998) J Phys Chem A 102:248
37. O'Malley PJ (1998) Chem Phys Lett 285:99
38. O'Malley PJ (1998) Chem Phys Lett 291:367
39. Lin T, O'Malley PJ (2011) J Phys Chem B 115:9311
40. Martin E, Samoilova RI, Narasimhulu KV, Lin T, O'Malley PJ, Wraight CA, Dikanov SA (2011) J Am Chem Soc 133:5525
41. Witwicki M, Jezierska J (2012) Geochim Cosmochim Acta 86:384
42. Improta R, Barone V (2004) Chem Rev 104:1231
43. Barone V, Cimino P (2009) J Chem Theory Comput 5:192
44. Ciofini I, Adamo C, Barone V (2004) J Chem Phys 121:6710
45. Condic-Jurkic K, Smith A, Hendrik Z, Smith DM (2012) J Chem Theory Comput 8:1078
46. Pauwels E, Declerck R, Verstraelen T, De Sterck B, Kay CWM, Van Speybroeck V, Waroquier M (2010) J Phys Chem B 114:16655
47. Witwicki M, Jezierska J (2011) J Phys Chem B 115:3172
48. Bennett IM, Farfano HMV, Bogani F, Primak A, Liddell PA, Otero L, Sereno L, Silber JJ, Moore AL, Moore TA, Gust D (2002) Nature 420:398
49. Bogeski I, Gulaboski R, Kappl R, Mirceski VB, Stefova M, Petreska J, Hoth M (2011) J Am Chem Soc 133:9293
50. Mirceski V, Gulaboski R, Bogeski I, Hoth M (2007) J Phys Chem C 111:6068
51. Yuasa J, Suenobu T, Fukuzumi S (2005) J Phys Chem A 109:9356
52. Ciofini I, Reviakine R, Arbuznikov A, Kaupp M (2004) Theor Chem Acc 111:132
53. Begue D, Carbonniere P, Barone V, Pouchan C (2005) Chem Phys Lett 416:206
54. Frisch MJ, Trucks GW, Schlegel HB, Scuseria GE, Robb MA, Cheeseman JR, Scalmani G, Barone V, Mennucci B, Petersson GA, Nakatsuji H, Caricato M, Li X, Hratchian HP, Izmaylov AF, Bloino J, Zheng G, Sonnenberg JL, Hada M, Ehara M, Toyota K, Fukuda R, Hasegawa J, Ishida M, Nakajima T, Honda Y, Kitao O, Nakai H, Vreven T, Montgomery JJA, Peralta JE, Ogliaro F, Bearpark M, Heyd JJ, Brothers E, Kudin KN, Staroverov VN, Kobayashi R, Normand J, Raghavachari K, Rendell A, Burant JC, Iyengar SS, Tomasi J, Cossi M, Rega N, Millam NJ, Klene M, Knox JE, Cross JB, Bakken V, Adamo C, Jaramillo J, Gomperts R, Stratmann RE, Yazyev O, Austin AJ, Cammi R, Pomelli C, Ochterski JW, Martin RL, Morokuma K, Zakrzewski VG, Voth GA, Salvador P, Dannenberg JJ, Dapprich S, Daniels AD, Farkas Ö, Foresman JB, Ortiz JV, Cioslowski J, Fox DJ (2009) Gaussian 09 revision A.02. Gaussian, Inc., Wallingford CT
55. Lee C, Yang W, Parr RG (1988) Phys Rev B 37:785
56. Becke AD (1993) J Chem Phys 98:1372
57. Stephens PJ, Devlin FJ, Chabalowski CF, Frisch MJ (1994) J Phys Chem 98:11623
58. Schaefer A, Horn H, Ahlrichs R (1992) J Chem Phys 97:2571
59. Barge A, Botta M, Casellato U, Tamburini S, Vigato PA (2005) Eur J Inorg Chem 2005:1492
60. Hewitt IJ, Tang JK, Madhu NT, Clérac R, Buth R, Anson CE, Powell AK (2006) Chem Commun 2650. http://pubs.rsc.org/en/content/articlelanding/2006/cc/b518026k
61. Akine S, Kagiyama S, Nabeshima T (2007) Inorg Chem 46:9525
62. Akine S, Taniguchi T, Nabeshima T (2006) J Am Chem Soc 128:15765
63. Cancès E, Mennucci B, Tomasi J (1997) J Chem Phys 107:3032
64. Tomasi J, Mennucci B, Cancès E (1999) J Mol Struct Theochem 464:211
65. Tomasi J, Mennucci B, Cammi R (2005) Chem Rev 105:2999
66. Neese F (2007) ORCA-an ab initio, DFT and semiempirical SCF-MO package, Version 2.6.35. University of Bonn, Germany
67. Adamo C, Barone V (1999) J Chem Phys 110:6158
68. Perdew JP, Burke K, Ernzerhof M (1996) Phys Rev Lett 77:3865
69. Becke AD (1988) Phys Rev A 38:3098
70. Perdew JP (1986) Phys Rev B 33:8822
71. Hoe W, Cohen A, Handy NC (2001) Chem Phys Lett 341:319
72. Klamt A, Schüürmann G (1993) J Chem Soc Perkin Trans 2:799
73. Sinnecker S, Rajendran A, Klamt A, Diedenhofen M, Neese F (2006) J Phys Chem A 110:2235
74. Neese F (2001) J Chem Phys 115:11080
75. Neese F (2005) J Chem Phys 122:34107

76. Bethe H, Salpeter E (1957) Quantum mechanics of one- and two-electron atoms. Springer, Berlin
77. Breit G (1929) Phys Rev 34:553
78. Dinadayalane TC, Hassan A, Leszczynski J (2012) Theor Chem Acc 131:1131
79. Russo N, Toscano M, Grand A (2003) J Phys Chem A 107:11533
80. Remko M, Rode BM (2006) J Phys Chem A 110:1960
81. Neese F (2009) Coord Chem Rev 253:526
82. Atanasov M, Comba P, Martin B, Muller V, Rajaraman G, Rohwer H, Wunderlich S (2006) J Comput Chem 27:1263
83. Tewary S, Gass IA, Murray KS, Rajaraman G (2013) Eur J Inorg Chem 2013:1024–1032
84. Stone AJ (1963) Mol Phys 6:509
85. Stone AJ (1964) Mol Phys 7:311
86. Schreckenbach G, Ziegler T (1997) J Phys Chem A 101:3388
87. Kaupp M, Bühl M, Malkin VG (2004) Calculation of nmr and epr parameters: theory and applications. Wiley-VCH, Weinheim
88. Baerend EJ, Autschbach J, Bashford D, Bérces A, Bickelhaupt FM, Bo C, Boerrigter PM, Cavallo L, Chong DP, Deng L, Dickson RM, Ellis DE, van Faassen M, Fan L, Fischer TH, Fonseca Guerra C, Ghysels A, Giammona A, van Gisbergen SJA, Götz AW, Groeneveld JA, Gritsenko OV, Grüning M, Harris FE, van den Hoek P, Jacob CR, Jacobsen H, Jensen L, van Kessel G, Kootstra F, Krykunov MV, van Lenthe E, McCormack DA, Michalak A, Mitoraj M, Neugebauer J, Nicu VP, Noodleman L, Osinga VP, Patchkovskii S, Philipsen PHT, Post D, Pye CC, Ravenek W, Rodríguez IJ, Ros P, Schipper PRT, Schreckenbach G, Seth M, Snijders JG, Solà M, Swart M, Swerhone D, te Velde G, Vernooijs P, Versluis L, Visscher L, Visser O, Wang F, Wesolowski TA, van Wezenbeek EM, Wiesenekker G, Wolff SK, Woo TK, Yakovlev AL, Ziegler T (2008) Amsterdam Density Functional (ADF) 2008.01, SCM, Theoretical Chemistry, Vrije Universiteit, Amsterdam, The Netherlands (http://www.scm.com)
89. Schreckenbach G, Ziegler T (1998) Theor Chem Acc 99:71
90. Atkins PW (1990) Physical chemistry, 4th edn. W. H. Freeman and Co., New York
91. Pearson RG (1963) J Am Chem Soc 85:3533